Available online at www.sciencedirect.com
ScienceDirect
Ceramics International 36 (2010) 2215–2220
CERAMICS INTERNATIONAL
www.elsevier.com/locate/ceramint

Sol–gel hydrothermal synthesis of bismuth–TiO_2 nanocubes for dye-sensitized solar cell

M.N. An'amt [a,*], S. Radiman [a], N.M. Huang [b,*], M.A. Yarmo [c], N.P. Ariyanto [d], H.N. Lim [e], M.R. Muhamad [b]

[a] School of Applied Physics, Faculty of Science & Technology, Universiti Kebangsaan Malaysia, 43600 Bangi, Selangor Darul Ehsan, Malaysia
[b] Low Dimensional Materials Research Centre, Block A, Physics Building, University of Malaya, 50603 Kuala Lumpur, Malaysia
[c] School of Chemical Science and Food Technology, Universiti Kebangsaan Malaysia, 43600 Bangi, Selangor Darul Ehsan, Malaysia
[d] Department of Electrical, Electronic & Systems Engineering, Faculty of Engineering and Build Environment, Universiti Kebangsaan Malaysia, 43600 Bangi, Selangor Darul Ehsan, Malaysia
[e] Faculty of Engineering, Nottingham University, Jalan Broga, 43500 Semenyih, Selangor, Malaysia

Received 11 March 2010; received in revised form 12 April 2010; accepted 14 May 2010
Available online 30 June 2010

Abstract

Bismuth–TiO_2 nanocubes were synthesized via a facile sol–gel hydrothermal method with titanium tetraisopropoxide as the precursor. The influence of the bismuth on the size, morphology, crystallinity and optical behavior of TiO_2 nanocubes were investigated. The samples were characterized by X-ray diffraction analysis (XRD), transmission electron microscopy (TEM), energy dispersive X-ray (EDX), field emission scanning electron microscopy (FESEM) and UV–visible spectroscopy (UV–vis). Photovoltaic behavior of dye-sensitized solar cells (DSSCs) fabricated using Bi–TiO_2 nanocubes was studied. The DSSCs had an open-circuit voltage (V_{oc}) of 590 mV, a short-circuit current density (J_{sc}) of 7.71 mA/cm^2, and the conversion efficiency (η) of 2.11% under AM 1.5 illumination, a 77% increment as compared to pure TiO_2 nanocubes.

Keywords: A. Sol–gel processing; B. Nanocomposites; D. TiO_2

1. Introduction

Titanium dioxide (TiO_2) is a wide band-gap semiconductor with energy of 3.0–3.2 eV. It is widely used in applications such as hydrogen production [1,2], gas sensors [3,4], photocatalytic activities [5,6], dye-sensitized solar cells and photoelectrochemical cells because of its relative high efficiency and high stability. However, due to its wide band gap energy, TiO_2 is active only under near-ultraviolet irradiation. Therefore, numerous researches have been carried out over the last 20 years to develop modified TiO_2 so that they are active under visible light irradiation ($\lambda > 400$ nm). One of the most studied methods is by doping the TiO_2 materials with metal ions (iron [7,8], nickel [9,10], vanadium [11,12], and chromium [13,14]) or nonmetallic elements (nitrogen [15,16], sulfur [17,18] and carbon [19,20]).

Among these doping methods, doping with transitional metals is one of the most efficient methods. Researches have been carried out to dope bismuth into TiO_2 to enhance the photocatalytic activities in these systems [21–24]. However, to the knowledge of the authors, there is no known report on the study of bismuth–TiO_2 nanomaterials for dye-sensitized solar cell (DSSC) application.

It has been reported that the metal/TiO_2 nanostructures will enhance the efficiency of DSSCs. Metals compounded on semiconductor materials increase charge-collection efficiency due to a much slower electron-hole recombination, giving rise to longer electron lifetime, which will result in an increasing interfacial electron-transfer process [25–27]. Metal–TiO_2 nanocomposites make an attractive research field by modifying the structure of the working electrode to improve the performance of solar energy conversion [28,29]. In DSSCs, the photoelectric conversion occurs by electron injection from photo-excited dye into the conduction band of TiO_2 and later the dye is regenerated by I^-/I_3^- through diffusion of electrons to the counter electrode [30,31]. Electron transport happens in

* Corresponding authors. Tel.: +60 38 9214256; fax: +60 38 9269470.
E-mail addresses: anamt_1003@yahoo.com (M.N. An'amt), huangnayming@gmail.com (N.M. Huang).

0272-8842/$36.00
doi:10.1016/j.ceramint.2010.05.027

the space charge region at nanocrystalline surface, which separates the photo-generated electron–hole and prevents charge recombination at the electrode–electrolyte interface. Decrease in probability of electron–hole recombination induces a large amount of electron–hole on the nanocrystalline surface, resulting in higher efficiency of solar energy conversion. Therefore, it is assumed that metal–TiO_2 nanocomposites could enhance the efficiency of DSSCs because of electron-transfer kinetics at the crystal surface and low probability of electron–hole recombination.

Hydrothermal approach has been used extensively for the synthesis of ceramic materials which takes advantage of a direct preparation at low crystallization temperatures [32–34]. In this work, we utilized Ti^{4+} aqueous solution to synthesis cube-like Bi–TiO_2 via sol–gel hydrothermal method. The Bi–TiO_2 nanocomposites formed were fabricated into DSSCs. To the best of our knowledge, this is the first report on the synthesis of Bi–TiO_2 nanocomposites for DSSCs application.

2. Experimental

2.1. Synthesis of TiO_2 and Bi–TiO_2 nanocubes

TiO_2 nanocrystals were synthesized using the modified sol–gel hydrothermal approach as reported previously [35]. In a typical synthesis route, 30 ml titanium tetraisopropoxide (TTIP) was added to 27 ml of triethanolamine (TEA) under constant magnetic stirring. Deionized water (18.2 MΩ cm resistivity) was added to obtain 200 ml of clear Ti^{4+} aqueous solution. Then, 30 ml of the Ti^{4+} solution was mixed with 30 ml of 0.1 M ethylenediamine. The mixed solution was then poured into a Teflon-lined autoclave and put inside the furnace at 100 °C for 24 h for gelation process. Then, the crystallization was completed by heating up the autoclave to 180 °C for 24 h. The hydrothermal crystallization time was varied for 24, 48 and 72 h at the same temperature with samples denoted as TiO_2-24, TiO_2-48 and TiO_2-72, respectively. Bi–TiO_2 nanocrystals were synthesized via the same procedure mentioned above with hydrothermal crystallization time of 72 h. The only difference was by adding 0.3 mmol $Bi(NO_3)_3{\cdot}5H_2O$ into the TTIP and TEA mixture during the initial stage of the synthesis process. All the samples were recovered by washing with deionized water followed by centrifugation for three times and dried at 60 °C in an oven overnight.

2.2. Fabrication of dye-sensitized solar cells (DSSCs)

In order to fabricate the DSSC, TiO_2 film electrode was made by the doctor blade technique on an indium tin oxide, ITO conductive glass (15 Ω cm resistivity). After drying in air and sintered at 450 °C for 30 min, the resulting film were immersed in an ethanol solution of 0.3 mM N_3 dye for about 16 h. The dye-adsorbed electrode was assembled into a sandwich-type cell with a counter electrode (platinum-sputtered ITO glass) and a spacer in the middle for ease of electrolyte solution injection. A drop of electrolyte solution (Iodolyte MPN-100, Solaronix) was introduced into the clamped electrodes using syringe. An active area typically 0.2 cm^2 was employed to measure the cell performance.

2.3. Characterization and DSSCs conversion efficiency measurement

The morphology and size of the samples were examined by a Philips CM12 transmission electron microscopy (TEM) operated at 100 kV. Measurement of the average diameter of the samples was carried out using an I-Solution-DT (version 6.5, IMT) image analysis software. A field emission scanning electron microscope, FESEM was used to examine the morphology of the sample and elemental analysis of the Bi–TiO_2 sample was carried out by energy dispersive analysis (EDX). The crystallinity of the samples were characterized by a Philip X-ray diffractometer (XRD) at a scanning rate of 0.02° s^{-1} with Cu Kα radiation and λ = 1.5418 Å. The optical properties were analyzed using a PerkinElmer Lamda-35 UV–vis spectrometer (UV–vis). The photovoltaic activities of the TiO_2 samples were measured by a Gamry Potentiostat Series G-300 under a xenon lamp, simulated solar illumination with Air Mass 1.5G filter (AM 1.5, 100 mW/cm^2).

3. Results and discussion

From Fig. 1, it was shown that the crystalline phase of the TiO_2 nanocrystals formed is anatase phase. There are no other peaks showing impurities or other TiO_2 phases like rutile or brookite present in the sample. The crystallinity and crystallite size increased as the hydrothermal treatment time increased based on the intensities of characteristic XRD peaks. All the peaks corresponded to the anatase phase of TiO_2 with 2θ = 25.3°, 36.9°, 37.8°, 36.6°, 48.0°, 53.8° and 55.0° attributed to [1 0 1], [1 0 3], [0 0 4], [1 1 2], [2 0 0], [1 0 5] and [2 1 1]

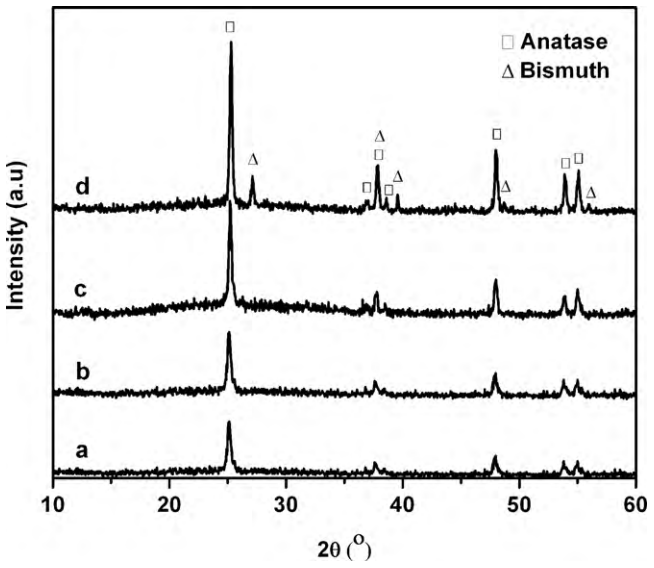

Fig. 1. XRD patterns of the TiO_2 nanocubes (a) TiO_2-24, (b) TiO_2-48, (c) TiO_2-72 and (d) Bi–TiO_2 prepared under different experimental conditions. The TiO_2 anatase peaks are labeled as square shape while the triangle shape denote peaks attributed to the Bi element.

plane, respectively (JCPDS 84-1285). When examining the diffraction peaks of Bi–TiO_2, it is clearly shown that there are other peaks besides the anatase phase. These peaks are indexed to the rombohedral phase of bismuth with $2\theta = 27.1^\circ$, 37.8°, 39.6°, 48.7° and 56.0° corresponding to [0 1 2], [1 0 4], [1 1 0], [2 0 2] and [0 2 4] plane, respectively (JCPDS 005-0519). It has been reported that the doping of bismuth into TiO_2 crystal structure can be observed from the shifting of 1 0 1 diffraction peak at $2\theta = 25.5^\circ$ [23]. For Bi doped sample, there will be a shift to lower angle because the ionic radius of Bi^{3+} (0.103 nm) is larger than that of Ti^{4+} (0.061 nm), the distance of nearest-neighbor crystalline plane becomes wider after Bi^{3+} ions replace Ti^{4+} ions in TiO_2. However, we do not observe this shifting phenomenon in our work; instead there is a slight shift towards the higher angle for Bi–TiO_2 sample. The slight shift towards the higher angle may be contributed by the mixed crystalline phases of anatase and bismuth metal. The inclusion of bismuth also increased the crystallinity of the TiO_2 nanocube crystals as can be seen from the intensity of the peaks. In general, the increase in the crystallinity of anatase TiO_2 is favorable to enhance the photovoltaic activity of TiO_2.

TEM micrographs in Fig. 2 show the morphologies of TiO_2 and Bi–TiO_2 nanocubes. The TiO_2 produced have cube-like shaped for all the different hydrothermal crystallization times and bismuth inclusion. As shown in Fig. 2(a–c), TiO_2-24, TiO_2-48 and TiO_2-72 have average sizes of 66 ± 18, 69 ± 11 and 75.2 ± 17 nm, respectively. This suggests that longer hydrothermal treatment allows particles to grow larger. While, Bi–TiO_2 nanocubes has the largest average particle size (92.3 ± 17 nm) as shown in Fig. 2(d). In comparison to the pure TiO_2 nanocubes, the Bi–TiO_2 nanocubes have higher reaction rate which contributed to the larger particle size produced. Fig. 3(a) shows a FESEM image of three-dimensional Bi–TiO_2 nanocubes which is in accordance to the observation from TEM while the atomic percentages of bismuth, titanium and oxygen were analyzed by EDX as shown in Fig. 3(b). For EDX, several areas on the individual nanocubes were selected for the analysis. It was found that the average atomic ratio for Ti:O is 32.4:65.1 which agrees well with the formation of TiO_2. The atomic percentage for bismuth is 1.5 wt.%. The EDX and XRD results have confirmed the existence of bismuth element on the surface of TiO_2 nanocubes instead of the doping of Bi^{3+}.

UV–vis absorption spectra for TiO_2-72 and Bi–TiO_2 were measured to study the effect of bismuth on optical property of TiO_2 nanocubes (Fig. 4). Undeniably, introduction of bismuth has modified the absorption characteristics of the TiO_2 nanocubes. It is obvious that the absorption range for Bi–TiO_2 have red shifted to longer wavelength which falls in the visible range as compared to TiO_2-72. This means that the Bi–TiO_2 sample can enlarge the wavelength response range and hence, enhances the solar light photovoltaic activity. This is crucial for TiO_2 material as the absorption region for TiO_2 falls in the UV zone which only consists of 5% in the solar light. The formation of Bi–TiO_2 nanocomposites intrinsically narrows the band-gap transition of TiO_2 which has the same effect as the reported Ag–TiO_2 nanocomposites [26,36,37].

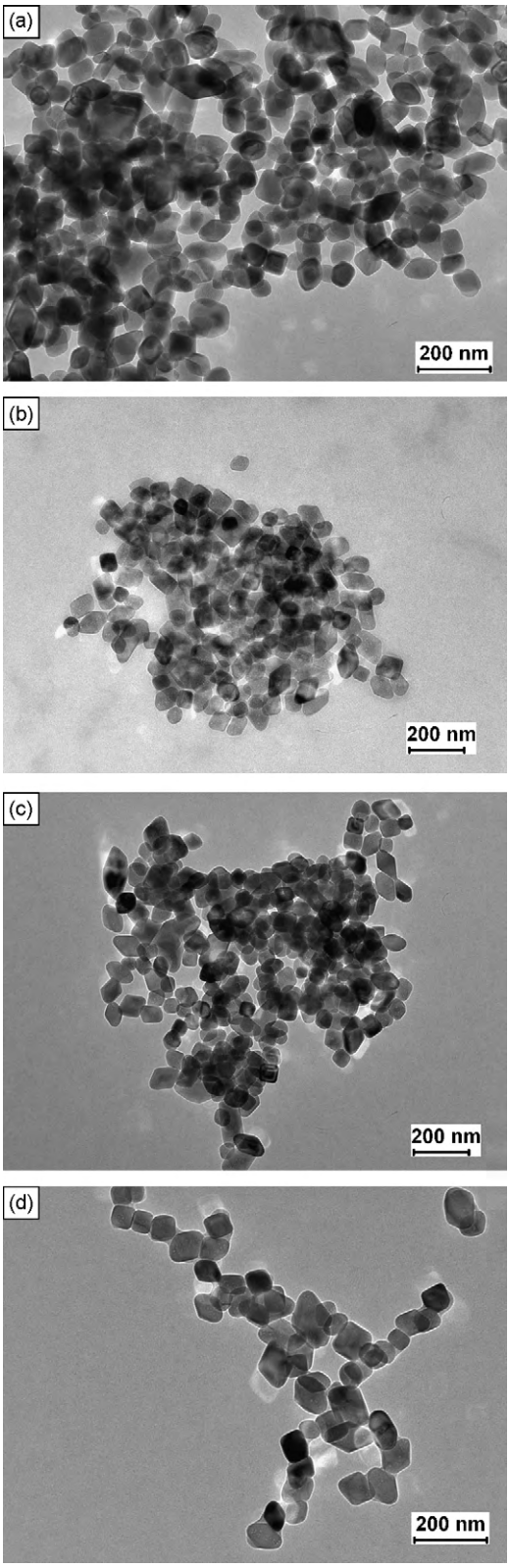

Fig. 2. TEM images of TiO_2 nanocubes (a) TiO_2-24, (b) TiO_2-48, (c) TiO_2-72 and (d) Bi–TiO_2 synthesized by the sol–gel hydrothermal method.

The photocurrent density–voltage characteristics (J–V curve) were studied under standard solar simulated light AM 1.5. From the analysis of the J–V curves, critical parameters of the cell's operation were obtained such as (a) open-circuit

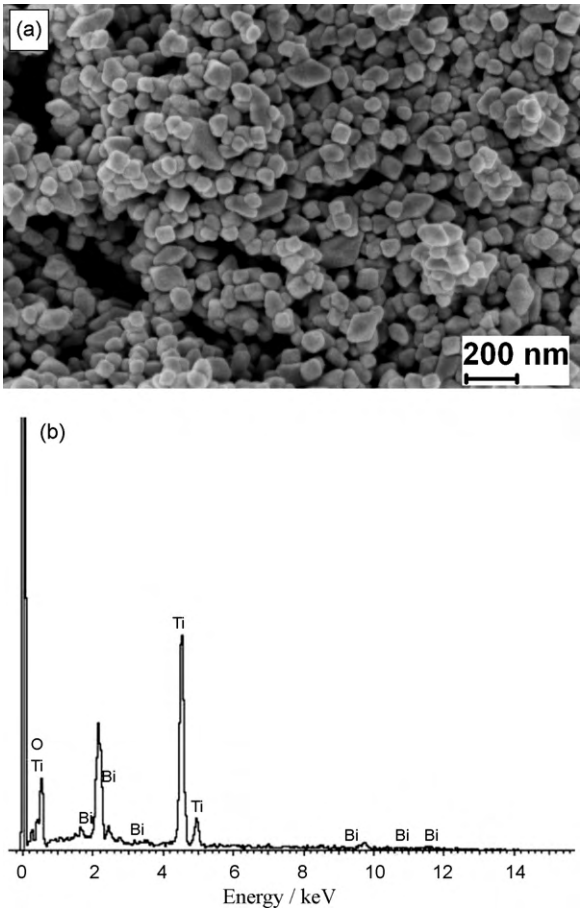

Fig. 3. FESEM image of cube-like Bi–TiO_2 (a) and EDX spectra of Bi–TiO_2 (b).

photovoltage V_{oc}, (b) the short-circuit photocurrent density J_{sc}, fill factor (FF) calculated using Eq. (1) and the cells overall energy conversion efficiency (η) estimated by Eq. (2). The parameters were shown in Table 1.

$$FF = \frac{V_{\max} J_{\max}}{V_{oc} J_{sc}} \quad (1)$$

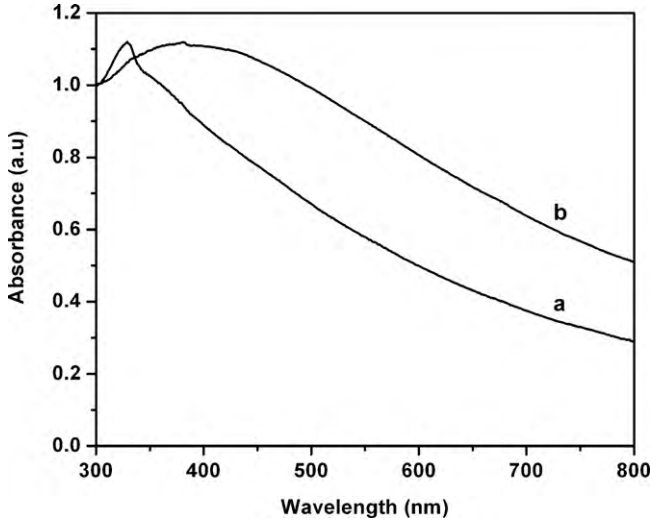

Fig. 4. UV–vis absorption spectra for (a) TiO_2-72 and (b) Bi–TiO_2 nanocubes.

Table 1
The critical parameters for open-circuit voltage (V_{oc}), short-circuit current density (J_{sc}), fill factor (FF) and cell efficiency (η) analyzed from curves J–V.

Electrode	V_{oc} (V)	J_{sc} (mA/cm^2)	FF (%)	η (%)
Bi–TiO_2	0.59	7.71	0.46	2.11
TiO_2-72	0.57	5.52	0.38	1.19
TiO_2-48	0.57	3.12	0.62	1.10
TiO_2-24	0.56	2.40	0.63	0.84

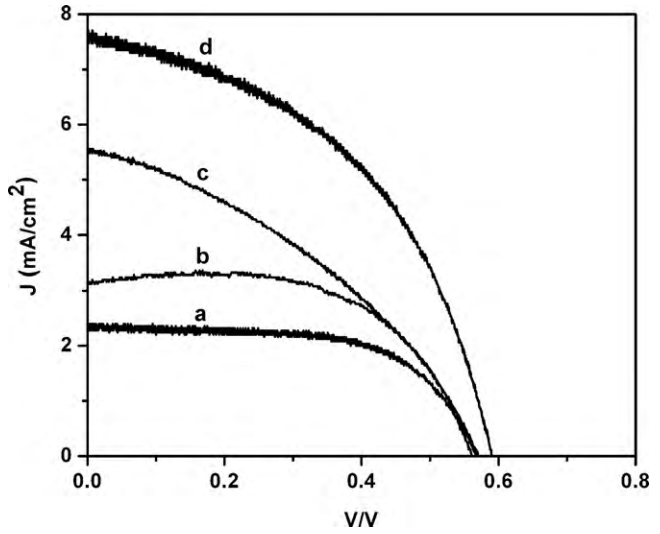

Fig. 5. Photocurrent density–voltage (J–V) curves for dye-sensitized solar cells using (a) TiO_2-24, (b) TiO_2-48, (c) TiO_2-72 and (d) Bi–TiO_2 nanocubes.

$$\eta = \frac{V_{oc} J_{sc} FF}{I_s} \quad (2)$$

where V_{max} and J_{max} are voltage and current density for maximum power output, respectively while I_s is the intensity of the incident light (mW/cm^2).

From the J–V curves results as shown in Fig. 5, a short-circuit photocurrent density (J_{sc}) of 7.71 mA/cm^2, an open-circuit photovoltage (V_{oc}) of 0.59 V and the conversion efficiency (η) of 2.11% for Bi–TiO_2 electrode were obtained. In comparison, J_{sc}, V_{oc}, and η were 5.52 mA/cm^2, 0.57 V, and 1.19%, respectively, for TiO_2-72 electrode. There is about 39% increase in J_{sc} and 77% increase in conversion efficiency for Bi–TiO_2 electrode compared to TiO_2-72 electrode, whereas η and V_{oc} for Bi–TiO_2 electrode are nearly the same as TiO_2-72 electrode. In this case, we have improved J_{sc} significantly without sacrificing V_{oc}, indicating that Bi–TiO_2 is better than TiO_2 for DSSCs with the same technique. For TiO_2-48 and TiO_2-24 electrodes, the J_{sc} and η values were lower than TiO_2-72 which is due to the shorter hydrothermal crystallization time as longer crystallization time resulted in higher crystallinity of the anatase phase formed. It has been reported that anatase phase with higher crystallinity resulted in lower probability of electron–hole recombination as the electron transport is faster in these anatase layer [16,17]. Furthermore, modification of the TiO_2 nanocubes' surface with bismuth has increased the charge transport and suppressed the electrons in TiO_2 to recombine

with the dye and redox species, and hence gives rise to the high DSSCs performance.

4. Conclusion

We report a facile sol–gel hydrothermal process to prepare Bi–TiO_2 nanocubes that demonstrated much higher dye-sensitized solar cell conversion efficiency than pure TiO_2. The enhanced DSSCs conversion efficiency for the Bi–TiO_2 sample is due to the formation of bismuth/TiO_2 nanocomposites and the higher crystallinity of the TiO_2 formed.

Acknowledgments

This work is supported by the UKM-OUP-NBT-27-138/2008 grant and UMRG grant RG096/10AFR. The author would like to thank Ms. Su and Mr. Hasnul from the Electron Microcopy Unit, UKM for their assistance in carrying out the EM characterization.

References

[1] W.S. Hong, J.H. Park, G.Y. Han, Optimization of conditions for hydrogen production from anodized TiO_2 nanotube-based photoelectrochemical cells, Journal of Nanoscience and Nanotechnology 9 (2009) 7293–7297.
[2] S. Sato, J.M. White, Photodecomposition of water over Pt/TiO_2 catalysts, Chemical Physics Letters 72 (1980) 83–86.
[3] C.-H. Han, D.-W. Hong, S.-D. Han, J. Gwak, K.C. Singh, Catalytic combustion type hydrogen gas sensor using TiO_2 and UV-LED, Sensors and Actuators B: Chemical 125 (2007) 224–228.
[4] J.A. Park, J. Moon, S.J. Lee, S.H. Kim, T. Zyung, H.Y. Chu, Structure and CO gas sensing properties of electrospun TiO_2 nanofibers, Materials Letters 64 (2010) 255–257.
[5] L.J. Chen, J.T. Tian, H. Qiu, Y.S. Yin, X. Wang, J.H. Dai, P.W. Wu, A.P. Wang, L. Chu, Preparation of TiO_2 nanofilm via sol–gel process and its photocatalytic activity for degradation of methyl orange, Ceramic International 35 (2009) 3275–3280.
[6] T. Yazawa, F. Machida, N. Kubo, T. Jin, Photocatalytic activity of transparent porous glass supported TiO_2, Ceramic International 35 (2009) 3321–3325.
[7] S. Nahar, K. Hasegawa, S. Kagaya, Photocatalytic degradation of phenol by visible light-responsive iron-doped TiO_2 and spontaneous sedimentation of the TiO_2 particles, Chemosphere 65 (2006) 1976–1982.
[8] X.W. Zhang, L.C. Lei, One step preparation of visible-light responsive Fe–TiO_2 coating photocatalysts by MOCVD, Materials Letters 62 (2008) 895–897.
[9] D.H. Kim, K.S. Lee, Y.S. Kim, Y.C. Chung, S.J. Kim, Photocatalytic activity of Ni 8 wt%-doped TiO_2 photocatalyst synthesized by mechanical alloying under visible light, Journal of the American Ceramic Society 89 (2006) 515–518.
[10] R. Niishiro, H. Kato, A. Kudo, Nickel and either tantalum or niobium-codoped TiO_2 and $SrTiO_3$ photocatalysts with visible-light response for H_2 or O_2 evolution from aqueous solutions, Physical Chemistry Chemical Physics 7 (2005) 2241–2245.
[11] S. Klosek, D. Raftery, Visible light driven V-doped TiO_2 photocatalyst and its photooxidation of ethanol, The Journal of Physical Chemistry B 105 (2001) 2815–2819.
[12] J.C.S. Wu, C.H. Chen, A visible-light response vanadium-doped titania nanocatalyst by sol–gel method, Journal of Photochemistry and Photobiology A: Chemistry 163 (2004) 509–515.
[13] S.K. Biswas, A. Pathak, N.K. Pramanik, D. Dhak, P. Pramanik, Codoped Cr and W rutile nanosized powders obtained by pyrolysis of triethanolamine complexes, Ceramic International 34 (2008) 1875–1883.
[14] C.C. Pan, J.C.S. Wu, Visible-light response Cr-doped $TiO_{2-X}N_X$ photocatalysts, Materials Chemistry and Physics 100 (2006) 102–107.
[15] J.L. Gole, J.D. Stout, C. Burda, Y.B. Lou, X.B. Chen, Highly efficient formation of visible light tunable $TiO_{2-x}N_x$ photocatalysts and their transformation at the nanoscale, Journal of Physical Chemistry B 108 (2004) 1230–1240.
[16] M. Mrowetz, W. Balcerski, A.J. Colussi, M.R. Hoffmann, Oxidative power of nitrogen-doped TiO_2 photocatalysts under visible illumination, The Journal of Physical Chemistry B 108 (2004) 17269–17273.
[17] Y.M. Liu, J.Z. Liu, Y.L. Lin, Y.F. Zhang, Y. Wei, Simple fabrication and photocatalytic activity of S-doped TiO_2 under low power LED visible light irradiation, Ceramic International 35 (2009) 3061–3065.
[18] Y. Wang, Y. Wang, Y. Meng, H. Ding, Y. Shan, X. Zhao, X. Tang, A highly efficient visible-light-activated photocatalyst based on bismuth- and sulfur-codoped TiO_2, The Journal of Physical Chemistry C 112 (2008) 6620–6626.
[19] T. Tachikawa, S. Tojo, K. Kawai, M. Endo, M. Fujitsuka, T. Ohno, K. Nishijima, Z. Miyamoto, T. Majima, Photocatalytic oxidation reactivity of holes in the sulfur- and carbon-doped TiO_2 powders studied by time-resolved diffuse reflectance spectroscopy, The Journal of Physical Chemistry B 108 (2004) 19299–19306.
[20] X. Yang, C. Cao, K. Hohn, L. Erickson, R. Maghirang, D. Hamal, K. Klabunde, Highly visible-light active C- and V-doped TiO_2 for degradation of acetaldehyde, Journal of Catalysis 252 (2007) 296–302.
[21] J. Wang, L. Jing, L. Xue, Y. Qu, H. Fu, Enhanced activity of bismuth-compounded TiO_2 nanoparticles for photocatalytically degrading rhodamine B solution, Journal of Hazardous Materials 160 (2008) 208–212.
[22] S. Rengaraj, X.Z. Li, Enhanced photocatalytic reduction reaction over Bi^{3+}–TiO_2 nanoparticles in presence of formic acid as a hole scavenger, Chemosphere 66 (2007) 930–938.
[23] T. Ji, F. Yang, Y. Lv, J. Zhou, J. Sun, Synthesis and visible-light photocatalytic activity of Bi-doped TiO_2 nanobelts, Materials Letters 63 (2009) 2044–2046.
[24] J. Yu, S. Liu, Z. Xiu, W. Yu, G. Feng, Combustion synthesis and photocatalytic activities of Bi^{3+}-doped TiO_2 nanocrystals, Journal of Alloys and Compounds 461 (2008) L17–L19.
[25] A. Sclafani, J.-M. Herrmann, Influence of metallic silver and of platinum-silver bimetallic deposits on the photocatalytic activity of titania (anatase and rutile) in organic and aqueous media, Journal of Photochemistry and Photobiology A: Chemistry 113 (1998) 181–188.
[26] M. Seery, K.R. George, P. Floris, S.C. Pillai, Silver doped titanium dioxide nanomaterials for enhanced visible light photocatalysis, Journal of Photochemistry and Photobiology A: Chemistry 189 (2007) 258–263.
[27] N. Sobana, M. Muruganadham, M. Swaminathan, Nano-Ag particles doped TiO_2 for efficient photodegradation of direct azo dyes, Journal of Molecular Catalysis A: Chemical 258 (2006) 124–132.
[28] C.-S. Chou, R.-Y. Yang, C.-K. Yeh, Y.-J. Lin, Preparation of TiO_2/nano-metal composite particles and their applications in dye-sensitized solar cells, Powder Technology 194 (2009) 95–105.
[29] Z. Liu, K. Pan, M. Liu, M. Wang, Q. Lü, J. Li, Y. Bai, T. Li, Al_2O_3-coated SnO_2/TiO_2 composite electrode for the dye-sensitized solar cell, Electrochimica Acta 50 (2005) 2583–2589.
[30] M. Grätzel, Dye-sensitized solar cells, Journal of Photochemistry and Photobiology C: Photochemistry Reviews 4 (2003) 145–153.
[31] B. O'Regan, M. Gratzel, A low-cost, high-efficiency solar cell based on dye-sensitized colloidal TiO_2 films, Nature 353 (1991) 737–740.
[32] D.S. Kim, S.-Y. Kwak, The hydrothermal synthesis of mesoporous TiO_2 with high crystallinity, thermal stability, large surface area, and enhanced photocatalytic activity, Applied Catalysis A: General 323 (2007) 110–118.
[33] H. Yan, X.-H. Zhang, J.-M. Wu, L.-Q. Wei, X.-G. Liu, B.-S. Xu, The use of CTAB to improve the crystallinity and dispersibility of ultrafine magnesium hydroxide by hydrothermal route, Powder Technology 188 (2008) 128–132.
[34] B. Bayati, A.A. Babaluo, R. Karimi, Hydrothermal synthesis of nanostructure NaA zeolite: the effect of synthesis parameters on zeolite seed size and crystallinity, Journal of the European Ceramic Society 28 (2008) 2653–2657.

[35] T. Sugimoto, X. Zhou, A. Muramatsu, Synthesis of uniform anatase TiO_2 nanoparticles by gel–sol method. 4. Shape control, Journal of Colloid and Interface Science 259 (2003) 53–61.
[36] H.M. Sung-Suh, J.R. Choi, H.J. Hah, S.M. Koo, Y.C. Bae, Comparison of Ag deposition effects on the photocatalytic activity of nanoparticulate TiO_2 under visible and UV light irradiation, Journal of Photochemistry and Photobiology A: Chemistry 163 (2004) 37–44.
[37] J. Wang, H. Zhao, X. Liu, X. Li, P. Xu, X. Han, Formation of Ag nanoparticles on water-soluble anatase TiO_2 clusters and the activation of photocatalysis, Catalysis Communications 10 (2009) 1052–1056.